

Residues Accessible in the Binding-Site Crevice of Transmembrane Helix 6 of the CB2 Cannabinoid Receptor[†]

Ntsang M. Nebane,[‡] Dow P. Hurst,[§] Carl A. Carrasquer,[‡] Zhuanhong Qiao,[‡] Patricia H. Reggio,[§] and Zhao-Hui Song^{*,‡}

Department of Pharmacology and Toxicology, University of Louisville School of Medicine, Louisville, Kentucky 40292, and Center for Drug Discovery, Department of Chemistry and Biochemistry, University of North Carolina at Greensboro, Greensboro, North Carolina 27402

Received May 1, 2008; Revised Manuscript Received October 16, 2008

ABSTRACT: We have used the substituted-cysteine accessibility method (SCAM) to map the residues in the sixth membrane-spanning segment of the CB2 cannabinoid receptor that contribute to the surface of the water-accessible binding-site crevice. Using a background of the mutant C2.59S which is relatively insensitive to the methanethiosulfonate (MTS) reagents, we mutated to cysteine, one at a time, 34 consecutive residues in TMH6 of the CB2 receptor. These mutant receptors were then expressed in HEK293 cells. By incubating HEK293 cells stably transfected with CB2 receptors with the small, charged, hydrophilic, thiol-specific reagent methanethiosulfonate ethylammonium (MTSEA), [³H]CP55940 binding was significantly inhibited for six mutant receptors. All six of the mutants that reacted with MTSEA were protected from the reaction when pretreated with the cannabinoid agonist WIN55212-2, suggesting that MTSEA modification occurred within the binding crevice. Therefore, the side chains of the residues at these reactive loci (V6.51, L6.52, L6.54, M6.55, L6.59, and T6.62) are on the water-accessible surface of the binding-site crevice. These residues are extracellular to the TMH6 CWXP hinge motif. The pattern of accessibility is consistent with a α -helical conformation for this segment of TMH6. Molecular modeling studies performed in the context of the CB2 model show that V6.51, L6.52, L6.54, M6.55, L6.59, and T6.62 face into the CB2 binding pocket, further confirming our SCAM results. These results are similar to the accessibility patterns determined by SCAM studies of TMH6 in the opioid and dopamine D2 receptors.

Cannabinoid receptors are members of the large family of G protein-coupled receptors (GPCRs).¹ To date, two cannabinoid receptors, CB1 and CB2, have been cloned. In 1990, a cDNA from a rat cerebral cortex cDNA library that encodes the first cannabinoid receptor subtype (CB1) was cloned (1). Subsequently, the sequences of an amino terminus variant CB1 receptor (2), as well as the human and mouse CB1 sequences, were reported (3, 4). The second cannabinoid receptor subtype, CB2, was first cloned in 1993 from a human promyelocytic leukemia cell HL60 cDNA library (5). The CB2 receptor in both rat (6, 7) and mouse (8) has been cloned as well. The CB1 receptor is located in the central nervous system as well as in the peripheral nervous system whereas the CB2 receptor has been found almost uniquely in immune cells (9–11). This distribution suggests a possible role for the CB2 receptor in mediating immunomodulatory but not psychoactive effects of cannabinoids, for which CB1 is the prime target. The human CB2 receptor exhibits 68% identity to the human CB1 receptor within the transmembrane regions and 44% identity throughout the whole protein (5).

CB1 and CB2 receptors couple to multiple signal transduction pathways, including adenylate cyclase (12, 13) and mitogen-activated protein kinase (14, 15).

The structure–function relationships and dynamics of protein activity can be studied using a combination of cysteine substitution and covalent modification (16). An extension of this combination, the substituted-cysteine accessibility method (SCAM), was first developed by Karlin and Akabas to map the channel-lining residues in the nicotinic acetylcholine receptor (17). Thereafter, this method was adapted to map the ligand binding crevice of dopamine D2 receptor, β 2-adrenergic receptor, opioid receptors, and other GPCRs (18–24). The development of SCAM (17) has proved to be a powerful tool to gain information about the structure and dynamics of protein domains and has been utilized to study not only G protein-coupled receptors (18–24) but also ligand-gated ion channels (25, 26), voltage-gated ion channels (27), and transporters (28). Javitch and co-workers have extensively studied the dopamine D2 receptor using the SCAM (18, 19, 21–23).

In the SCAM method, after establishing an appropriate background in which all reactive native cysteines are mutated

[†] This work was supported in part by National Institutes of Health Grants DA11551 and EY13632 to Z.-H.S. and Grants DA03934 and KO5 DA021358 to P.H.R.

* To whom correspondence should be addressed. E-mail: zhsong@louisville.edu. Phone: 502-852-5160. Fax: 502-852-7868.

[‡] University of Louisville School of Medicine.

[§] University of North Carolina at Greensboro.

¹ Abbreviations: GPCR, G protein-coupled receptor; HEK293, human embryonic kidney cells; MTS reagents, methanethiosulfonate reagents; MTSEA, methanethiosulfonate ethylammonium; Rho, rhodopsin; SCAM, substituted-cysteine accessibility method; TMH, transmembrane helix.

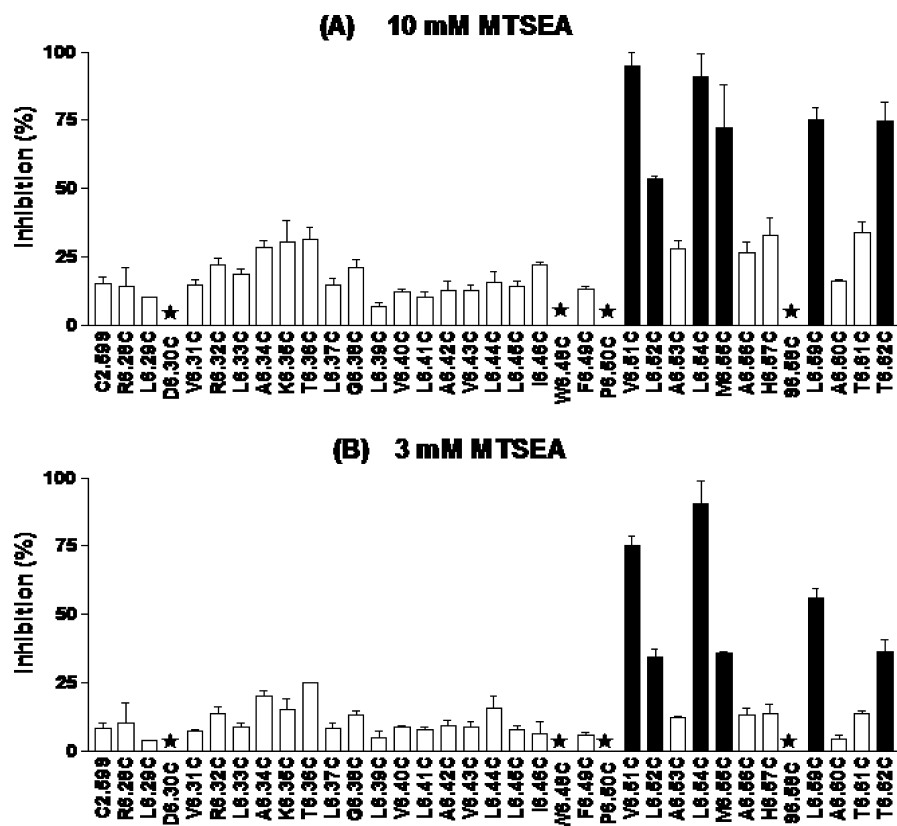


FIGURE 2: Effects of MTSEA on specific [3 H]CP55940 binding to mutant CB2 receptors. HEK293 cells stably transfected with C2.59S background and CB2 cysteine-substitution mutant receptors were treated with 3 and 10 mM MTSEA for 10 min at room temperature. CP55940 was then used for competition binding with [3 H]CP55940 on the MTSEA-treated cells. Data shown represent the means \pm SEM of at least six independent experiments performed in duplicate. Solid black bars are mutants for which inhibition was significantly different ($p < 0.05$) from the background by one-way ANOVA plus Newman-Keul's post test. The stars signify mutants for which [3 H]CP55940 binding was undetected.

ence were treated with 1.5 μ g of wild-type or mutant receptor cDNA in 10 μ L of lipofectamine and 1 mL of OPTIMEM. Stably transfected cells were selected in culture medium containing 800 μ g/mL Geneticin. Having established cell lines stably expressing wild-type and mutant CB2 receptors, the cells were maintained in growth medium containing 400 μ g/mL Geneticin until needed for experiments.

Cell Harvesting. Cells were washed twice with phosphate-buffered saline (PBS) containing 8.1 mM NaH_2PO_4 , 1.5 mM KH_2PO_4 , 138 mM NaCl, and 2.7 mM KCl, pH 7.2, and then dissociated in PBS containing 1 mM EDTA. Dissociated cells were collected by centrifugation at 1000g for 5 min at 4 $^\circ\text{C}$. The cell pellets were resuspended in binding buffer (50 mM Tris-HCl, 200 mM sucrose, 5 mM MgCl_2 , 2.5 mM EDTA, and 0.5 mg/mL bovine serum albumin, pH 7.4) for treatment with MTSEA and ligand binding assays.

Treatment with MTSEA. MTSEA was always freshly prepared by dissolving in distilled water at 4 $^\circ\text{C}$. Aliquots (180 μ L) of the cell suspensions were incubated with 20 μ L of MTSEA at the stated concentrations for 10 min at room temperature. Cell suspensions were then diluted 50-fold with binding buffer and centrifuged at 1000g for 5 min. After the supernatant was discarded, the cell pellets were resuspended in binding buffer for ligand binding assays.

Protection by WIN55212-2 against MTSEA Reaction. For the ligand binding crevice protection experiments, the cells expressing C2.59S background and cysteine-substitution mutant CB2 receptors were preincubated with cannabinoid ligand WIN55212-2 at two different concentrations (0.1 and

1 μ M) for 40 min and then treated with MTSEA for 10 min at a concentration that causes $>80\%$ inhibition of ligand binding. After diluting with binding buffer and centrifuging at 1000g for 5 min at 4 $^\circ\text{C}$, the cell pellets were resuspended in fresh binding buffer and incubated for 15 min at room temperature. Thereafter, the cell pellets were again centrifuged at 1000g for 5 min at room temperature, resuspended in fresh binding buffer, and incubated for 15 min at room temperature. This process was repeated eight times to wash off the cannabinoid ligands. At the end of washing, the cells were resuspended in binding buffer for ligand binding assays. Protection was calculated as $1 - [(\text{inhibition of binding in the presence of WIN55212-2})/(\text{inhibition in the absence of drug})]$.

Ligand Binding Assay. Cannabinoid ligand dilutions were made in binding buffer and then added to silanized assay tubes. [3 H]CP55940 was used as radiolabeled ligand for competition binding assays. Nonspecific binding was determined in the presence of 1 μ M unlabeled CP55940. Binding assays were performed in 0.5 mL of binding buffer containing 0.1 mg/mL BSA for 60 min at 30 $^\circ\text{C}$. Cells were incubated with unlabeled CP55940 in binding buffer in the presence of [3 H]CP55940. Free and bound radioligands were separated by rapid filtration through GF/B filters. The filters were washed three times with 3 mL of cold wash buffer (50 mM Tris-HCl, pH 7.4, consisting of 1 mg/mL BSA). The bound [3 H]CP55940 was determined by liquid scintillation counting after overnight equilibration in 5 mL of scintillation fluid (CytoScint; ICN, Costa Mesa, CA). The assays were

performed in duplicate, and the results represent the combined data from at least three independent experiments.

Determination of Second-Order Rate Constant. The second-order rate constant (k_{MTSEA}) for the reaction of MTSEA with wild-type CB2 or each mutant was estimated according to the method used by Javitch and co-workers (19). In brief, each receptor was incubated with different concentrations of MTSEA for a fixed time. The results were fit to the equation $Y = (1 - \text{plateau})e^{-kct} + \text{plateau}$. Y is the fraction of initial binding, plateau is the fraction of residual binding at saturating concentrations of MTSEA, k is the second-order rate constant ($\text{M}^{-1} \text{s}^{-1}$), c is the concentration of MTSEA (molar), and t is the fixed time (seconds). This equation was transformed into the following form: $-\ln[(Y - \text{plateau})/(1 - \text{plateau})]/t = kc$. After plotting $-\ln[(Y - \text{plateau})/(1 - \text{plateau})]/t$ against c , k was obtained as the slope.

Data Analysis. Data from ligand binding assays were analyzed and curves generated by using the GraphPad Prism program (GraphPad Software). The IC_{50} and EC_{50} values were determined through nonlinear regression analysis performed with Prism. K_d values were estimated from competition binding experiments using the equation $K_d = \text{IC}_{50} - L$, where L is the concentration of the total radioligand (34).

Computer Model of CB2 Transmembrane Helix Bundle. A model of CB2 was created using the 2.8 Å crystal structure of bovine rhodopsin (Rho) (35) as a starting point. Model creation began with an alignment of the bovine Rho and human CB2 sequences. Fourier transform methods were employed to guide the alignment of sequences in the TMH5 region, as CB2 lacks the highly conserved Pro residue normally used as the alignment guide in this sequence region (36). Changes to the general Rho structure that were necessitated by sequence divergences included (1) the absence of helix kinking proline residues in TMH1 and TMH5, (2) a structural role for S2.54(84) due to the lack of a GG motif in TMH2 (31), and (3) the possible difference in flexibility of TMH6 (37). Complete details of the creation of our transmembrane helix model of CB2 are provided in our recent publication (31). Below we describe the addition of loop segments and N- and C-termini to this TMH bundle model to complete our model of CB2.

Modeling of Loops and N- and C-Termini. (A) *Initial Construction and Refinement.* Extracellular (EC-1 H(98)–S(102); EC-2 W(172)–N(188); EC-3 L(273)–K(278)) and intracellular (IC-1 H(62)–K(67); IC-2 P(138)–L(145); IC-3 A(216)–G(233)) loops, as well as the N- (M(1)–S(29)) and C-termini (H(316)–C(360)) were added to the refined CB2 TMH bundle model using the Loopy program within the protein structure modeling suite, Jackal 1.5 (J. Z. Xiang and B. Honig, Columbia University). The Modeler program was then used to refine loop structures (38, 39).

(B) *Special Considerations for EC-2 Loop.* The EC-2 loop (W172–N188) is the largest extracellular loop in CB2. The conformation of this loop was calculated using the biased scaled collective variable in Monte Carlo (SCV-MC) method (40, 41). The aqueous environment of the EC-2 loop was modeled with a recently developed implicit solvent model that is based on a screened Coulomb potential formulation (the SCP-ISM) (42, 43). This loop has an internal C4.66(174)–C179 disulfide bridge, one which has been suggested to be present in CB2 via mutagenesis studies (44).

(C) *Special Considerations for IC-3 Loop.* NMR experiments on a peptide fragment comprised of the CB1 sequence span from the intracellular end of TMH5 to the intracellular end of TMH6 in micelles suggested that sections of the CB1 IC-3 loop are α -helical (45). These regions consist in a short α -helical segment from A301 to R307 followed by an elbow region (R307–I309) and an α -helical segment (Q310–S316) up to a Ile-Ile-Ile (I317–I319) in IC-3. The initial portion of the CB2 IC-3 loop (AHQHVAS) bears high homology with the analogous sequence in the CB1 IC-3 loop (AHSHAVR) that Ulfers and co-workers found to be helical, while the rest of the IC-3 loops are quite divergent between CB2 and CB1. On the basis of these results, we replaced the initial Loopy built IC-3 loop with an intracellular α -helix (A216–S222). The rest of the IC-3 loop (L223–G233) was then rebuilt using Loopy and optimized using Modeler.

Final Energy Minimization. The energy of the CB2 transmembrane helix bundle model was minimized using the OPLS 2005 force field in Macromodel 9.1 (Schrödinger Inc., Portland, OR). An 8.0 Å extended nonbonded cutoff (updated every 10 steps), 20.0 Å electrostatic cutoff, and 4.0 Å hydrogen bond cutoff were used in each stage of the calculation. The minimization was performed in two steps. The first step consisted of conjugate gradient minimization in a distance-dependent dielectric until a gradient of 0.1 kcal/mol was reached. This stage of the calculation allowed the helix bundle to pack. To preserve the pitch of the transmembrane helices during this minimization, a 100 kcal/mol restraint was placed on all ϕ and ψ angles in TMHs 1–7 and Hx 8. N- and C-termini together with extra- and intracellular loops were then added to the minimized TMH bundle model as described above.

In the second stage of the calculation, the added loop and termini regions were allowed to relax during a 500 step Polak–Ribier conjugate gradient (PRCG) minimization. The transmembrane helix bundle atoms were defined as non-moving fixed atoms, but their nonbonded contributions to the system were retained as implemented in Macromodel. The loop and termini regions were unrestrained. An 8.0 Å extended nonbonded cutoff (updated every 10 steps), 20.0 Å electrostatic cutoff, and 4.0 Å hydrogen bond cutoff were used in this calculation, and the generalized Born/surface area (GB/SA) continuum solvation model for water available in Macromodel was employed.

Measurements of TMH Geometry. The bend, wobble, and face shifts of transmembrane helices were measured using Simulaid (46).

RESULTS

Ligand Binding Assay. Effects of Cysteine Substitution on Agonist Binding. MTSEA has been shown to be the most effective MTS reagent for inhibition of ligand binding to the CB2 cannabinoid receptor (31). We therefore used MTSEA in this study. Using the background of the C2.59(89)S mutant which is relatively insensitive to MTSEA (31), we mutated to cysteine, one at a time, 34 consecutive residues, R6.28–T6.62 of TMH6. The cysteine-substituted mutants as well as the background mutant were stably expressed in HEK293 cells and the K_d values characterizing the equilibrium binding of the radiolabeled agonist, [^3H]CP55940, determined. The K_d values ranged from 0.58 to 19.79 nM

Table 1: Parameters of [³H]CP55940 Binding to Wild-Type and TMH6 Cysteine-Substituted CB2 Receptors Stably Expressed in HEK293 Cells^a

	K_d (95% CI) (nM)	$K_d^{mut}/K_d^{C2.59S}$	B_{max} (fmol)/ 10 ⁴ cells	n
CB2	8.98 (5.60–14.39)	0.4	3.13 ± 0.35	6
C2.59S	22.90 (17.23–30.44)	1.0	7.84 ± 0.05	10
R6.28C	7.29 (2.95–18.61)	0.32	2.97 ± 0.29	6
L6.29C	10.79 (6.35–18.34)	0.47	6.40 ± 0.05	6
D6.30C	ND ^b			6
V6.31C	2.25 (1.37–3.70) ^c	0.10	4.34 ± 0.07	6
R6.32C	4.33 (2.40–7.82) ^c	0.20	5.53 ± 0.10	6
L6.33C	1.29 (0.90–1.86) ^c	0.06	2.41 ± 0.07	6
A6.34C	1.54 (1.00–2.36) ^c	0.07	3.04 ± 0.08	6
K6.35C	1.31 (0.83–2.08) ^c	0.06	1.99 ± 0.40	6
T6.36C	0.58 (0.40–0.82) ^c	0.03	1.06 ± 0.04	6
L6.37C	5.10 (3.26–7.89) ^c	0.22	2.42 ± 0.04	6
G6.38C	5.18 (3.97–6.74) ^c	0.23	2.35 ± 0.08	6
L6.39C	5.51 (3.09–9.84) ^c	0.24	2.08 ± 0.05	6
V6.40C	3.61 (2.45–5.33) ^c	0.16	1.75 ± 0.30	6
L6.41C	19.79 (9.84–39.80)	0.86	7.50 ± 0.80	6
A6.42C	13.55 (7.58–24.20)	0.59	7.08 ± 0.29	6
V6.43C	12.83 (6.78–24.26)	0.56	6.64 ± 0.17	6
L6.44C	9.93 (5.04–19.58)	0.43	4.18 ± 0.08	6
L6.45C	9.56 (5.48–16.69) ^c	0.42	4.47 ± 0.15	6
I6.46C	2.72 (1.86–3.99) ^c	0.12	3.07 ± 0.04	6
W6.48C	ND			6
F6.49C	8.57 (4.25–17.29)	0.37	4.26 ± 0.09	6
P6.50C	ND			6
V6.51C	10.97 (3.35–35.88)	0.48	5.09 ± 0.21	6
L6.52C	1.31 (0.93–1.84) ^c	0.06	2.13 ± 0.40	6
A6.53C	8.06 (4.43–14.66) ^c	0.35	3.48 ± 0.06	6
L6.54C	0.99 (0.52–1.87) ^c	0.04	1.73 ± 0.08	6
M6.55C	2.12 (1.05–4.29) ^c	0.09	2.51 ± 0.11	6
A6.56C	8.02 (4.45–14.45) ^c	0.35	3.04 ± 0.11	6
H6.57C	7.78 (4.69–12.90) ^c	0.34	3.17 ± 0.08	6
S6.58C	ND			6
L6.59C	3.73 (2.23–6.23) ^c	0.16	2.15 ± 0.08	6
A6.60C	8.55 (4.27–17.14) ^c	0.37	3.51 ± 0.07	6
T6.61C	3.50 (2.12–5.76) ^c	0.15	2.33 ± 0.20	6
T6.62C	1.58 (1.00–2.48) ^c	0.07	2.49 ± 0.06	6

^a K_d and B_{max} values were measured in competition binding experiments using [³H]CP55940 as radioligand (see Experimental Procedures). Data are the mean ± SEM of at least six independent experiments performed in duplicate. ^b ND, no detectable binding. ^c Significantly different from the background (C2.59S) ($p < 0.05$).

(Table 1). All but eight of the cysteine-substitution mutants had K_d values significantly lower than that of the C2.59S background mutant. For the eight mutants R6.28C, L6.29C, L6.41C, A6.42C, V6.43C, L6.44C, F6.49C, and V6.51C, K_d values were not significantly different from that of the C2.59S mutant. K_d values could not be determined for D6.30C, W6.48C, P6.50C, and S6.58C, which lacked detectable binding.

Reactions of MTSEA with the Mutants. MTSEA at 10 mM significantly inhibited [³H]CP55940 binding to 6 of 31 cysteine-substitution mutants (Figure 2A). MTSEA at 3 mM also significantly blocked binding to these six mutants, to different extents (Figure 2B).

Determination of Second-Order Rate Constant. To quantify the susceptibility of MTSEA, we determined the second-order rate constants for the sensitive mutants (Table 2 and Figure 3). The rate constants of the mutant receptors (V6.51C, L6.52C, L6.54C, M6.55C, L6.59C, and T6.62C) were 4–6 times higher than that of the background (C2.59S) mutant receptor but comparable to that of the wild-type CB2 receptor. To confirm the difference between sensitive and insensitive mutants, we also calculated the second-order rate constants for several insensitive mutants for which [³H]CP55940 binding was not significantly inhibited by

MTSEA. The second-order rate constants for these mutants (T6.36C, H6.57C, and T6.61C) were no different from that of the C2.59S background mutant.

Protective Effect of WIN55212-2 against the Inhibitory Action of MTSEA. To determine whether the substituted cysteine residues that reacted with MTSEA are actually within or in the vicinity of the binding pockets, we examined if the CB2 receptor agonist WIN55212-2 could protect the substituted cysteines from the inhibitory action of MTSEA on [³H]CP55940 binding. The residues that constitute the surface of the binding-site crevice are a subset of the water-accessible residues. Pretreatment of MTSEA-sensitive cysteine-substituted mutants with WIN55212-2 significantly reduced the inhibitory effects of MTSEA on [³H]CP55940 binding for all of the sensitive mutants, including V6.51C, L6.52C, L6.54C, M6.55C, L6.59C, and T6.62C (Figure 4). The extent of protection varied for different mutants, with the higher WIN55212-2 concentration of 1 μ M generally affording more protection than 0.1 μ M WIN55212-2.

Molecular Modeling. SCAM results reported here suggest that residues V6.51, L6.52, L6.54, M6.55, L6.59, and T6.62 are accessible to MTSEA from within the binding-site crevice. Figure 5A illustrates the positions of these residues in the context of the CB2 model reported here. It is clear here that V6.51, L6.54, M6.55, L6.59, and T6.62 face into the CB2 binding pocket. While the C- α -C- β bond of residue L6.52 is in the TMH6–TMH5 interface of the CB2 model, the Leu side chain points into the binding-site crevice when its χ -1 torsion angle is in g^+ (as illustrated in Figure 5A). In addition, the flexibility of TMH6 may contribute to residue L6.52 being accessible to the binding-site crevice.

Thus the modeling and SCAM studies reported here are in direct agreement with each other. Figure 5 also illustrates the positions of the same residues in the three reported crystal structures of class A GPCRs (bovine rhodopsin (Figure 5B) (35), human β -2-adrenergic (β -2-AR; Figure 5C) (47, 48), and turkey β -1-adrenergic (β -1-AR; Figure 5D)) (49) receptors. It is clear here that the residues labeled in CB2 would be accessible in these other receptors as well. Figure 5 also illustrates a fundamental difference between the position of the extracellular end of TMH6 in the CB2 model vs rhodopsin, β -2-AR and β -1-AR. The origin of this difference is explored in the Discussion section.

DISCUSSION

Effects of Cysteine Substitution on [³H]CP55940 Binding. In this study, 22 of the cysteine-substitution mutants had K_d values lower than that of the C2.59S background mutant. These mutations therefore increased [³H]CP55940 binding affinity for the CB2 cannabinoid receptor. The rest of the cysteine-substitution mutants (R6.28C, L6.29C, L6.41C, A6.42C, V6.43C, L6.44C, F6.49C, and V6.51C) had K_d values for [³H]CP55940 not significantly different from that of the C2.59S background mutant. [³H]CP55940 was used in this study because a suitable radiolabeled CB2 antagonist is currently not available to us. One possible complication with all mutagenesis experiments is that the overall structure of the mutant receptors may be changed from the wild-type receptor structure. However, in this study, because the majority of the cysteine mutations caused either no change in the K_d value for CP55940 or decreased the K_d value, we

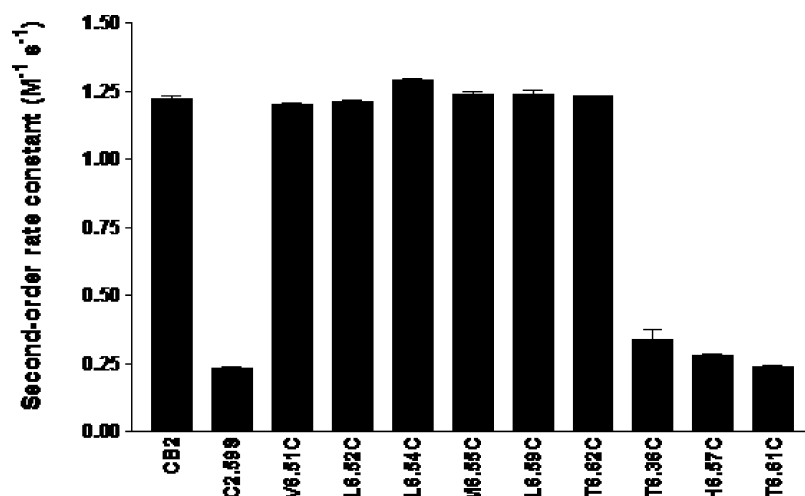


FIGURE 3: Comparison of second-order rate constants for wild-type CB2, C2.59S background mutant, and CB2 TMH6 cysteine-substitution mutant receptors. The experiments were performed as described in Experimental Procedures. Data shown represent the means \pm SEM of at least six independent experiments performed in duplicate.

Table 2: Rates of Reaction of MTSEA ($M^{-1} s^{-1}$) with Cysteine-Substitution Mutants of the CB2 Receptor Stably Expressed in HEK293 Cells^a

receptor	k_{MTSEA} ($M^{-1} s^{-1}$)	k_{MUT}/k_{WT}
CB2*	1.22 ± 0.03	1.00
C2.59S	0.23 ± 0.03	0.19
(T6.36C)	0.34 ± 0.09	0.28
V6.51C*	1.20 ± 0.02	0.98
L6.52C*	1.21 ± 0.02	0.99
L6.54C*	1.29 ± 0.02	1.06
M6.55C*	1.24 ± 0.03	1.02
(H6.57C)	0.28 ± 0.01	0.23
L6.59C*	1.24 ± 0.03	1.02
(T6.61C)	0.24 ± 0.01	0.20
T6.62C*	1.23 ± 0.01	1.01

^a Second-order rate constants were determined as described in Experimental Procedures. Cells were treated with four concentrations of MTSEA (1, 3, 10, and 30 mM), and [³H]CP55940 binding was performed. Rate constants of all accessible mutants were determined. Data represent the means \pm SEM of at least four independent experiments performed in duplicate. k_{MUT}/k_{WT} was obtained by dividing the k value obtained for each cysteine mutant by the k value of the CB2 wild-type receptor (not the C2.59S background which does not react). The asterisk denotes a statistically significant difference ($p < 0.05$) compared to the C2.59S background mutant by one-way ANOVA plus Newman–Keul’s post test. The parentheses show selected “insensitive” mutants that were not significantly more inhibited than the background (C2.59S) mutant.

believe that the overall structures of the mutant receptors are not compromised by the cysteine substitutions. Since TMH6 is the key helix involved in GPCR activation (50), it is possible that those mutations led to higher binding affinities (lowered K_d values) that might have biased receptor populations toward activated state, thus increasing agonist affinity.

W6.48, D6.30, P6.50, and S6.58. Even though W6.48C, D6.30C, P6.50C, and S6.58C receptor proteins were detected on cell membranes by Western blot analysis (data not shown), these mutant receptors lost their ability to bind [³H]CP55940. W6.48, D6.30, and P6.50 are highly conserved residues whereas S6.58 is not a conserved amino acid among GPCRs.

In opioid receptors, the W6.48C mutation did not alter [³H]diprenorphine binding affinity (24). In the dopamine D2 receptor, the W6.48C mutant showed greatly reduced binding affinity (21). W6.48 is a highly conserved residue in rhodopsin-like GPCRs and is part of the very important

CWXP hinge motif in TMH6 of class A GPCRs. Mutating W6.48 of the CB1 cannabinoid receptor to alanine resulted in a significant reduction in ligand binding affinity in the presence of WIN55212-2 and SR141716A but not CP55940 and anandamide (51). In our recent mutagenesis studies on the CB2 receptor, W6.48A and W6.48F mutant receptors completely lost their ligand binding and signaling ability (52). These results, together with our W6.48C mutant binding results, suggest that a tryptophan residue at position 6.48 is important for ligand binding and proper function of CB2 receptor. This tryptophan at 6.48 may be necessary to maintain the proper geometry of the ligand binding pocket.

There has been no report on a D6.30C mutation for either the opioid or the dopamine D2 receptors. Previously, we have shown that the D to N mutation at position D6.30 of the CB2 receptor did not result in a loss of ligand binding (53). Residue 6.30 is part of an intracellular ionic lock (with R3.50/D3.49) in rhodopsin (35). The CB2 D6.30N mutant would retain the ability to hydrogen bond with R3.50 and may be the reason why the D6.30N mutation does not show deleterious effects on ligand binding. The D6.30C mutation may cause this connection with R3.50 to be lost, given that Cys residues are not strong hydrogen-bonding residues. This may explain the deleterious effect of D6.30C mutation on ligand binding seen in this study.

In the D2 dopamine receptor, P6.50C reduced the binding affinity of the antagonist [³H]-N-methylspiperone to the receptor (21). Similar to our P6.50C results, [³H]diprenorphine binding was undetectable for P6.50C mutants of the μ , δ , and κ opioid receptors in SCAM studies by Xu and co-workers (24). Our results suggest that the 6.50 locus is crucial for maintaining ligand binding and function of the CB2 receptor. P6.50 is the most conserved residue in TMH6 and is responsible for the helix kink. It might be expected that a P6.50C mutant would exhibit no binding given that this mutation will cause a drastic change in TMH6 geometry.

The S6.58C mutant lost ligand binding ability. S6.58 is an important residue at the extracellular end of TMH6 in CB2. Modeling studies suggest that this residue hydrogen bonds with EC-3 loop residues D(275) and S(274) and stabilizes the position of the extracellular end of TMH6. Because Cys has reduced hydrogen-bonding tendency, the

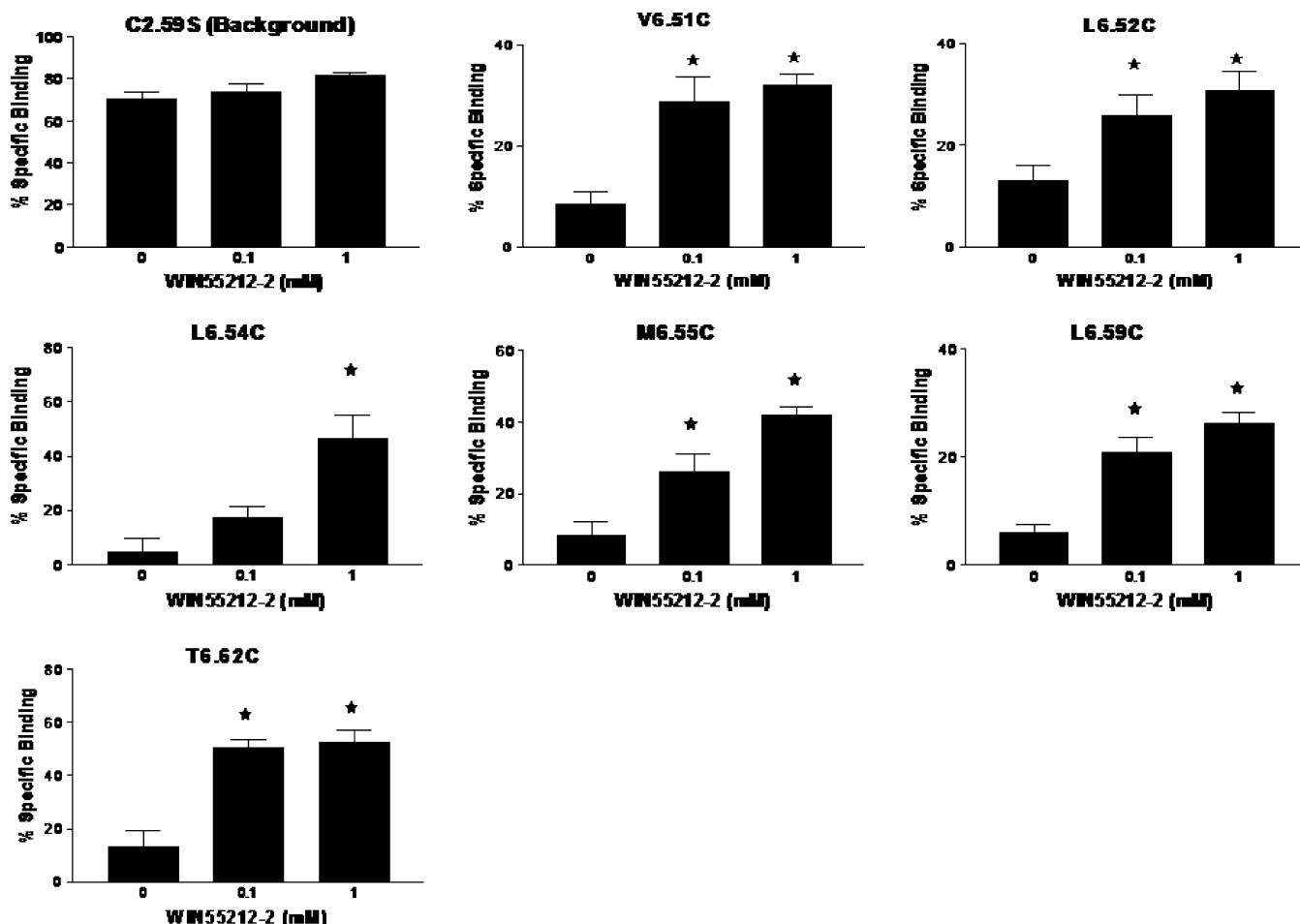


FIGURE 4: WIN55212-2 protection of the MTSEA effects on specific [^3H]CP55940 binding to mutant CB2 receptors. HEK293 cells stably transfected with C2.59S background and cysteine-substitution mutant receptors were incubated without or with 0.1 and 1 μM WIN55212-2 for 40 min at 30 $^{\circ}\text{C}$ and then reacted with 10 mM (V6.51C and L6.54C) or 30 mM (L6.52C, M6.55C, L6.59C and T6.62C) MTSEA (to inhibit >80% of binding) for 10 min at room temperature. The cells were then washed eight times, resuspended in binding buffer, and assayed for specific [^3H]CP55940 binding as described under Experimental Procedures. The data are expressed as a fraction of the binding measured in the absence of MTSEA treatment. Data shown represent the means \pm SEM of at least four independent experiments performed in quadruplet. WIN55212-2 provided significant protection ($p < 0.05$ *) by one-way ANOVA plus Newman–Keul's post test for all of the mutants.

S6.58C mutation may result in a destabilization of the extracellular position of TMH6, perturbing receptor structure and resulting in loss of ligand binding.

Residues in TMH6 That Are Accessible in the Binding-Site Crevice. Several mechanisms can possibly explain the inhibition of ligand binding when an MTS reagent reacts with an accessible cysteine. These include steric block, electrostatic repulsion, and/or an indirect structural effect on the binding site. Our SCAM results show that [^3H]CP55940 binding to 6 out of 30 mutants in TMH6 was sensitive to MTSEA. Cannabinoids are well-known for their hydrophobic properties. WIN55212-2 was used for protection experiments, because among all the cannabinoids that we tested, this compound is the easiest to wash off in protection assays. WIN55212-2 protected the binding of [^3H]CP55940 from the inhibitory action of MTSEA for all of these sensitive cysteine mutants. WIN55212-2 could protect directly substituted cysteine residues on the surface of the binding pocket from reaction with MTSEA, as well as protect substituted cysteine residues deeper in the binding-site crevice by blocking the passage of MTSEA from the extracellular medium. The residues identified by our results as being on the water-accessible surface of the binding-site crevice of the CB2 receptor include V6.51, L6.52, L6.54, M6.55, L6.59,

and T6.62. As is clear in Figure 5, these residues form an arc that describes the degree to which the extracellular portion of TMH6 is pushed into the TMH bundle.

The loss of binding to the four cysteine-substitution mutants (W6.48C, D6.30C, P6.50C, and S6.58C) suggests that the structures of these mutant receptors, especially around the binding site, have probably been distorted by the mutation such that the substituted cysteine no longer lies in an orientation similar to that of the wild-type receptor. Two of the mutant residues that lost their ligand binding ability (W6.48C and S6.58C) are predicted by modeling studies reported here to face into the binding-site crevice. W6.48 of the μ and κ opioid receptors and K6.58, W6.58, and E6.58, respectively, of the μ , δ , and κ opioid receptors (24) were also identified as being in the water-accessible binding-site crevice. P6.50 is predicted by modeling to face the lipid, and mutation of this residue to Cys can be expected to introduce structural perturbations in the TMH bundle. P6.50 was not identified as being in the water-accessible crevice of the μ , δ , and κ opioid receptors (24); however, this residue could be labeled in the dopamine D2 receptor (21). The other CB2 residue which lost its binding (D6.30C) is located at the intracellular end of TMH6 and therefore would not have been available for modification by MTSEA.

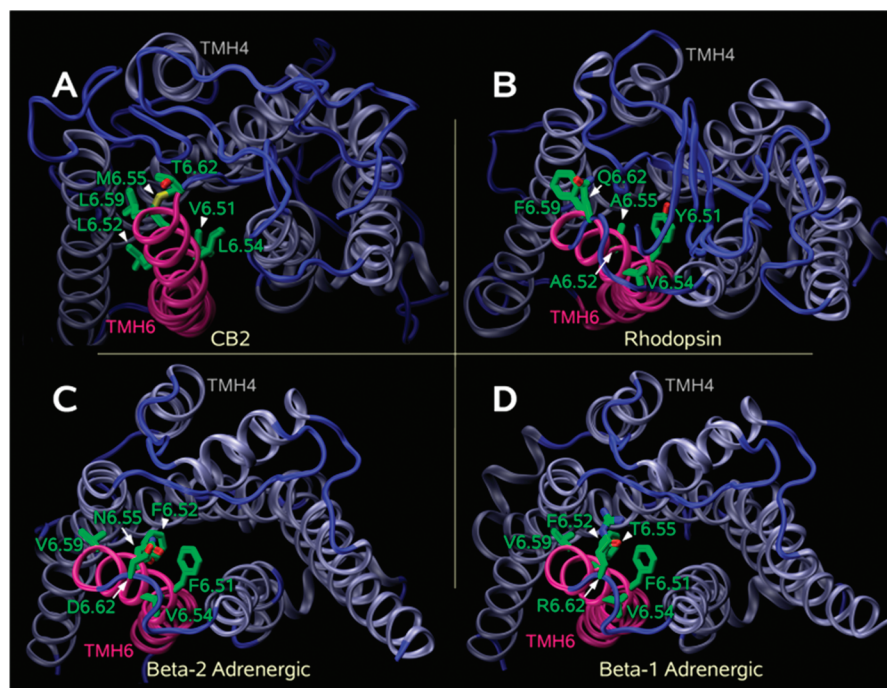


FIGURE 5: Extracellular views of receptor models. (A) An extracellular view of the CB2 model. This model includes both N- and C-termini, as well as extracellular and intracellular loops. TMH6 is highlighted in magenta, and the residues labeled by MTSEA (V6.51, L6.52, L6.54, M6.55, L6.59, and T6.62) are highlighted in green. (B–D) Illustrated here are the positions of these same residues in the three reported crystal structures of the class A GPCRs: bovine rhodopsin (panel B) (35), the human β -2-adrenergic (β -2-AR; panel C) (47, 48), and the turkey β -1-adrenergic (β -1-AR; panel D) (49) receptors. It is clear that the residues labeled by MTSEA in CB2 would be accessible in these other receptors as well.

Most of the residues identified in our study as being on the water-accessible surface of the binding-site crevice of CB2 were also found to be accessible in the μ , δ , and κ opioid receptors, as well as in the dopamine D2 receptor. Just like our results for V6.51, L6.54, M6.55, and L6.59, Xu and co-workers (24) identified I6.51, Y6.54, V6.55, and A6.59 of the μ receptor, I6.51, F6.54, V6.55, and T6.59 of the δ receptor, and I6.51, F6.54, I6.55, and A6.59 of the κ receptor as being on the water-accessible surface of the binding-site crevice. Javitch and co-workers (21) identified F6.51, F6.52, T6.54, H6.55, and I6.59 of the dopamine D2 receptor, residues which we also identified in CB2 as being on the water-accessible surface of the binding-site crevice. Three of their residues, V6.40, F6.44, and I6.56, were insensitive to MTSEA in our studies. Unlike ours, their W6.48C did not lose binding and was accessible in the binding-site crevice of the dopamine D2 and the μ and κ opioid receptors but not in the δ opioid receptor. H6.52C, which showed no detectable binding for all three opioid receptors, was identified as being on the water-accessible surface of the binding-site crevice of CB2, just like F6.52 of the dopamine D2 receptor. CB2 residue 6.62 was also labeled in the work reported here. Modeling studies predict that residue 6.62 is not part of TMH6 but is at the beginning of the EC-3 loop. However, this residue does face the ligand binding pocket (Figure 5), and this is likely the reason why this residue was reactive to MTSEA.

Rate Constants of MTSEA Reaction. The second-order rate constants of the sensitive cysteine mutants were similar in magnitude. There was, however, a 4–6-fold significant ($p < 0.05$) difference between the rate constants of the sensitive and insensitive mutants, signifying that the reaction of MTSEA with cysteines in the binding-site crevice is accelerated approximately 4–6-fold. This increase in second-

order rate constants between the most reactive CB2 TMH6 residue and the least reactive residue, though statistically significant, is much less than the 100-fold increase in second-order rate constants reported for the μ , κ , and δ opioid receptors (24) or the dopamine D2 receptor (21).

There is one important structural difference in CB2 that may contribute to the lower MTSEA reactivity rates seen. Class A GPCRs such as rhodopsin, β -2-AR, and β -1-AR have a Cys in the EC-2 loop and a Cys at 3.25 that form a disulfide bridge. As evidenced in the bovine rhodopsin (35), human β -2-AR (47, 48), and turkey β -1-AR (49) crystal structures, this disulfide bridge causes the EC-2 loop region C-terminal to the conserved disulfide bond to be deeper in the binding-site crevice than is the N-terminal part of the EC-2 loop. The position of the EC-2 loop in each of these structures is illustrated in Figure 6B–D. Here the EC-2 loop is colored green and shown in molecular surface display (probe radius = 1.4 Å). It is clear here that, in each case, the EC-2 loop protrudes into the binding-site crevice between TMH3 and TMH6. This protrusion will limit how close the TMH bundle can pack together. At the same time, this protrusion will not block water penetration into the binding-site crevice but actually will facilitate such penetration since the TMH bundle is prevented from closer packing with itself. Shi and Javitch found that the pattern of accessibility of EC-2 loop residues in the dopamine D2 receptor was consistent with a structure similar to that of bovine rhodopsin. These investigators concluded that the EC-2 loop likely contributes to the binding site in the D2 receptor (54). While no EC-2 loop SCAM studies have been reported for the opioid receptors, each of these receptors also has a Cys in the EC-2 loop and a Cys at residue 3.25. Thus the structure of the opioid receptors in the EC-2 loop region is likely to be similar to rhodopsin, the β -2-adrenergic, the β -1-adrenergic, and the

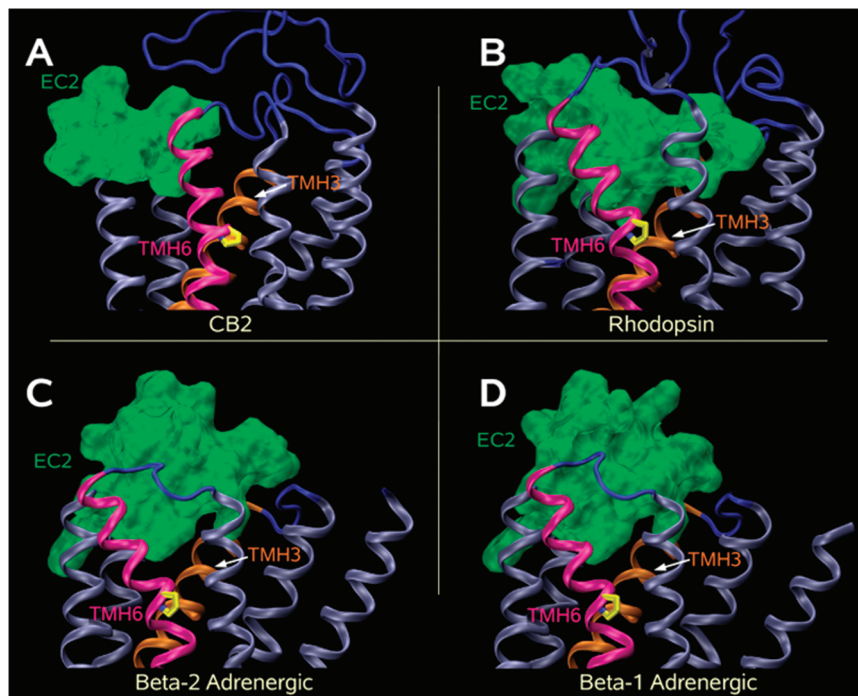


FIGURE 6: EC-2 loop positions and penetration into the binding pocket. The differences in EC-2 loop penetration into the binding pockets of (A) CB2, (B) bovine rhodopsin (35), (C) the human β -2-AR (47, 48), and (D) the turkey β -1-AR (49) are illustrated here. Class A GPCRs such as rhodopsin, β -2-AR, and β -1-AR (but not CB2) have a Cys in the EC-2 loop and a Cys at 3.25 that form a disulfide bridge. In (B) the bovine rhodopsin (35), (C) the human β -2-AR (47, 48), and (D) the turkey β -1-AR (49) crystal structures, this disulfide bridge causes the EC-2 loop region C-terminal to the conserved disulfide bond to be deeper in the binding-site crevice than is the N-terminal part of the EC-2 loop. Here the EC-2 loop is colored green and shown in molecular surface display (probe radius = 1.4 Å). It is clear that in panels B–D the EC-2 loop protrudes into the binding-site crevice between TMH3 and TMH6. This protrusion will limit how close the TMH bundle can pack together. In contrast, the CB2 receptor (A) lacks the Cys at 3.25. It is likely that an internal EC-2 C4.66(174)–C179 disulfide bridge (44) forms in CB2. Because the CB2 EC-2 loop does not have as deep a penetration into the binding pocket, the CB2 TMH bundle can more closely pack with itself, likely resulting in decreased water penetration, as well as a slowing of MTSEA reaction kinetics even for residues higher in the binding-site crevice.

dopamine D2 receptors. In contrast to these other class A GPCRs, the CB2 receptor lacks the Cys at 3.25 and therefore cannot mimic these other receptors. It is likely that an internal EC-2 C4.66(174)–C179 disulfide bridge (44) forms in CB2. Modeling studies suggest that because the CB2 EC-2 loop does not penetrate as deeply into the binding pocket (see Figure 6A), the CB2 TMH bundle can more closely pack with itself. One of the effects of this increased packing may be diminished water penetration and therefore reduced ability to label residues deeper in the binding pocket, as well as a slowing of MTSEA reaction kinetics even for residues higher in the binding-site crevice.

Geometry of TMH6. The pattern of residues in TMH6 of the CB2 cannabinoid receptor accessible in the binding-site crevice is consistent with TMH6 having an α -helical conformation extracellular to P6.50 (37) (Figure 5). These results are consistent with TMH6 residues found to be accessible to the binding site by SCAM studies of the dopamine D2 receptor (21) and the μ , δ , and κ opioid receptors (24).

The difference in the EC-2 loop between CB2 and rhodopsin, β -2-AR, and β -1-AR (Figure 6) may also impact the direction in which the extracellular portion of TMH6 points. Figure 5 shows that the TMH6 wobble angle in the CB2 model causes the extracellular end of TMH6 to point into the TMH bundle toward TMH4 (Figure 5A), while the extracellular end of TMH6 in rhodopsin, β -2-AR, or β -1-AR actually points out of the bundle past TMH5 (Figure 5B–D). This is reflected in the wobble angles for TMH6 in

bovine rhodopsin (35), human β -2-AR (47, 48), and turkey β -1-AR (49) and the model of human CB2 which are -83.7° , -73.0° , -65.5° , and -121.6° , respectively. The much larger magnitude wobble angle for CB2 TMH6 is possible because the EC-2 loop in CB2 does not penetrate deeply into the binding pocket, enabling the top of TMH6 to occupy a region precluded by the EC-2 loop in rhodopsin, β -2-AR, and β -1-AR.

CONCLUSIONS

In this study, we used the substituted cysteine accessibility method to identify novel CB2 receptor binding-site residues and to elucidate the secondary structure of TMH6 of CB2. The cannabinoid agonist WIN55212-2 protected V6.51, L6.52, L6.54, M6.55, L6.59, and T6.62 from modification by the MTS reagent, indicating that these six residues line the CB2 binding site. Our molecular modeling studies indicate that these same six residues face into the CB2 binding pocket (V6.51, L6.52, M6.55, L6.54, L6.59, and T6.62), thereby corroborating our SCAM studies.

REFERENCES

1. Matsuda, L. A., Lolait, S. J., Brownstein, M. J., Young, A. C., and Bonner, T. I. (1990) Structure of a cannabinoid receptor and functional expression of the cloned cDNA. *Nature* 346, 561–564.
2. Shire, D., Carillon, C., Kaghad, M., Calandra, B., Rinaldi-Carmona, M., and Le Fur, G. (1995) An amino-terminal variant of the central cannabinoid receptor resulting from alternative slicing. *J. Biol. Chem.* 270, 3726–3731.

3. Gerard, C. M., Mollereau, C., Vassart, G., and Parmentier, M. (1991) Molecular cloning of a human brain cannabinoid receptor which is also expressed in testis. *Biochem. J.* 279, 129–134.
4. Abood, M. E., Ditto, K. E., Noel, M. A., Showalter, V. M., and Tao, Q. (1997) Isolation and expression of a mouse CB1 cannabinoid receptor gene. Comparison of binding properties with those of native CB1 receptors in mouse brain and N18TG2 neuroblastoma cells. *Biochem. Pharmacol.* 53, 207–214.
5. Munro, S., Thomas, K. L., and Abu-Shaar, M. (1993) Molecular characterization of a peripheral receptor for cannabinoids. *Nature* 365, 61–65.
6. Griffin, G., Tao, Q., and Abood, M. (2000) Cloning and pharmacological characterization of the rat CB2 cannabinoid receptor. *J. Pharmacol. Exp. Ther.* 292, 886–894.
7. Brown, S. M., Wager-Miller, J., and Mackie, K. (2002) Cloning and molecular characterization of the rat CB2 cannabinoid receptor. *Biochim. Biophys. Acta* 1576, 255–264.
8. Shire, D., Calandra, B., Rinaldi-Carmona, M., Oustric, D., Pessegue, B., Bonnin-Cabanne, O., Le Fur, G., Caput, D., and Ferrara, P. (1996) Molecular cloning, expression and function of the murine CB2 peripheral cannabinoid receptor. *Biochim. Biophys. Acta* 1307, 132–136.
9. Pertwee, R. G. (1997) Pharmacology of cannabinoid CB1 and CB2 receptors. *Pharmacol. Ther.* 74, 129–180.
10. Buckley, N. E., Hansson, S., Harta, G., and Mezey, E. (1998) Expression of the CB1 and CB2 receptor messenger RNAs during embryonic development in the rat. *Neuroscience* 82, 1131–1149.
11. Friedman, H., Klein, T. W., Newton, C., and Daaka, Y. (1995) Marijuana, receptors and immunomodulation. *Adv. Exp. Med. Biol.* 373, 103–113.
12. Felder, C. C., Joyce, K. E., Briley, E. M., Mansouri, J., Mackie, K., Blond, O., Lai, Y., Ma, A. L., and Mitchell, R. L. (1995) Comparison of the pharmacology and signal transduction of the human CB1 and CB2 receptors. *Mol. Pharmacol.* 48, 443–450.
13. Glass, M., and Felder, C. C. (1997) Concurrent stimulation of cannabinoid CB1 and dopamine D2 receptors augments cAMP accumulation in striatal neurons: Evidence for a G_s-linkage to the CB1 receptor. *J. Neurosci.* 17, 5327–5333.
14. Bouaboula, M., Poinot-Chazel, C., Bourrié, B., Canat, X., Calandra, B., Rinaldi-Carmona, M., Le Fur, G., and Casellas, P. (1995) Activation of mitogen activated protein kinases by stimulation of the central cannabinoid receptor CB1. *Biochem. J.* 312, 637–641.
15. Bouaboula, M., Poinot-Chazel, C., Marchand, J., Canat, X., Bourrié, B., Rinaldi-Carmona, M., Calandra, B., Le Fur, G., and Casellas, P. (1996) Signaling pathway associated with stimulation of CB2 peripheral cannabinoid receptor: involvement of both mitogen-activated protein kinase and induction of Krox-24 expression. *Eur. J. Biochem.* 237, 704–711.
16. Farrens, D. L., Altenbach, C., Yang, K., Hubbell, W. L., and Khorana, H. G. (1996) Requirement of rigid-body motion of transmembrane helices for light activation of rhodopsin. *Science* 274, 768–770.
17. Karlin, A., and Akabas, M. H. (1998) Substituted-cysteine accessibility method. *Methods Enzymol.* 293, 123–145.
18. Javitch, J. A., Li, X., Kaback, J., and Karlin, A. (1994) A cysteine residue in the third membrane-spanning segment of the human D2 dopamine receptor is exposed in the binding-site crevice. *Proc. Natl. Acad. Sci. U.S.A.* 91, 10355–10359.
19. Javitch, J. A., Fu, D., and Chen, J. (1995) Residues in the fifth membrane-spanning segment of the dopamine D2 receptor exposed in the binding-site crevice. *Biochemistry* 34, 16433–16439.
20. Javitch, J. A., Fu, D., Liapakis, G., and Chen, J. (1997) Constitutive activation of the beta2 adrenergic receptor alters the orientation of its sixth membrane-spanning segment. *J. Biol. Chem.* 272, 18546–18549.
21. Javitch, J. A., Ballesteros, J. A., Weinstein, H., and Chen, J. (1998) A cluster of aromatic residues in the sixth membrane-spanning segment of the dopamine D2 receptor is accessible in the binding-site crevice. *Biochemistry* 37, 998–1006.
22. Javitch, J. A., Ballesteros, J. A., Chen, J., Chiappa, V., and Simpson, M. M. (1999) Electrostatic and aromatic microdomains within the binding-site crevice of the D2 receptor: contributions of the second membrane-spanning segment. *Biochemistry* 38, 7961–7968.
23. Javitch, J. A., Shi, L., Simpson, M. M., Chen, J., Chiappa, V., Visiers, I., Weinstein, H., and Ballesteros, J. A. (2000) The fourth transmembrane segment of the dopamine D2 receptor: accessibility in the binding-site crevice and position in the transmembrane bundle. *Biochemistry* 39, 12190–12199.
24. Xu, W., Li, J., Chen, C., Huang, P., Weinstein, H., Javitch, J. A., Shi, L., de Riel, J. K., and Liu-Chen, L. Y. (2001) Comparison of the amino acid residues in the sixth transmembrane domains accessible in the binding-site crevices of mu, delta, and kappa opioid receptors. *Biochemistry* 40, 8018–8029.
25. Akabas, M. H., and Karlin, A. (1995) Identification of acetylcholine receptor channel-lining residues in the M1 segment of the alpha-subunit. *Biochemistry* 34, 12496–12500.
26. Beck, C., Wollmuth, L. P., Seeburg, P. H., Sakmann, B., and Kuner, T. (1999) NMDAR channel segments forming the extracellular vestibule inferred from the accessibility of substituted cysteines. *Neuron* 22, 559–570.
27. Koch, S. E., Bodi, I., Schwartz, A., and Varadi, G. (2000) Architecture of Ca²⁺ channel pore-lining segments revealed by covalent modification of substituted cysteines. *J. Biol. Chem.* 275, 34493–34500.
28. Lambert, G., Forster, I. C., Stange, G., Kohler, K., Biber, J., and Murer, H. (2001) Cysteine mutagenesis reveals novel structure-function features within the predicted third extracellular loop of the type IIa Na(+)/P(i) cotransporter. *J. Gen. Physiol.* 117, 533–546.
29. Roberts, D. D., Lewis, S. D., Ballou, D. P., Olson, S. T., and Shafer, J. A. (1986) Reactivity of small thiolate anions and cysteine-25 in papain toward methyl methanethiosulfonate. *Biochemistry* 25, 5595–5601.
30. Ballesteros, J. A., and Weinstein, H. (1995) Integrated methods for the construction of three dimensional models and computational probing of structure function relations in G protein-coupled receptors, in *Methods in Neuroscience* (Conn, P. M., and Sealfon, S. C., Eds.) Vol. 25, Chapter 19, pp 366–428.
31. Zhang, R., Hurst, D. P., Barnett-Norris, J., Reggio, P. H., and Song, Z. H. (2005) Cysteine 2.59(89) in the second transmembrane domain of human CB2 receptor is accessible within the ligand binding crevice: evidence for possible CB2 deviation from a rhodopsin template. *Mol. Pharmacol.* 68, 69–83.
32. Song, Z. H., and Bonner, T. I. (1996) A lysine residue of the cannabinoid receptor is critical for receptor recognition by several agonists but not WIN55212-2. *Mol. Pharmacol.* 49, 891–896.
33. Song, Z. H., Slowey, C. A., Hurst, D. P., and Reggio, P. H. (1999) The difference between the CB(1) and CB(2) cannabinoid receptors at position 5.46 is crucial for the selectivity of WIN55212-2 for CB(2). *Mol. Pharmacol.* 56, 834840.
34. DeBlasi, A., O'Reilly, K., and Motulsky, H. J. (1989) Calculating receptor number from binding experiments using same compound as radioligand and competitor. *Trends Pharmacol. Sci.* 10, 227–229.
35. Palczewski, K., Kumasaka, T., Hori, T., Behnke, C. A., Motoshima, H., Fox, B. A., Le Trong, I., Teller, D. C., Okada, T., Stenkamp, R. E., Yamamoto, M., and Miyano, M. (2000) Crystal structure of rhodopsin: A G protein-coupled receptor. *Science* 289, 739–745.
36. Bramblett, R. D., Panu, A. M., Ballesteros, J. A., and Reggio, P. H. (1995) Construction of a 3D model of the cannabinoid CB1 receptor: determination of helix ends and helix orientation. *Life Sci.* 56, 1971–1982.
37. Barnett-Norris, J., Hurst, D. P., Buehner, K., Ballesteros, J. A., Guarnieri, F., and Reggio, P. H. (2002) Agonist alkyl tail interaction with cannabinoid CB1 receptor V6.43/I6.46 groove induces a helix 6 active conformation. *Int. J. Quantum Chem.* 88, 76–86.
38. Sali, A., and Blundell, T. L. (1993) Comparative protein modelling by satisfaction of spatial restraints. *J. Mol. Biol.* 234, 779–815.
39. Fiser, A., Do, R. K., and Sali, A. (2000) Modeling of loops in protein structures. *Protein Sci.* 9, 1753–1773.
40. Hassan, S. A., Mehler, E. L., and Weinstein, H. (2002) Structure calculation of protein segments connecting domains with defined secondary structure: A simulated annealing Monte Carlo combined with biased scaled collective variables technique, in *Computational Methods for Macromolecules: Challenges and Applications* (Schlick, T., and Gan, H. H., Eds.) pp 197–231, Springer Verlag, New York.
41. Barnett-Norris, J., Hurst, D. P., and Reggio, P. H. (2003) The influence of cannabinoid receptor second extracellular loop conformation on the binding of CP55940, in *2003 Symposium on the Cannabinoids*, p 79, International Cannabinoid Research Society, Cornwall, Ontario.
42. Hassan, S. A., Guarnieri, F., and Mehler, E. L. (2000b) A general treatment of solvent effects based on screened Coulomb potentials. *J. Phys. Chem. B* 104, 6478–6489.
43. Hassan, S. A., Guarnieri, F., and Mehler, E. L. (2000) Characterization of hydrogen bonding in a continuum solvent model. *J. Phys. Chem. B* 104, 6490–6498.

44. Gouldson, P., Calandra, B., Legoux, P., Kerneis, A., Rinaldi-Carmona, M., Barth, F., Le Fur, G., Ferrara, P., and Shire, D. (2000) Mutational analysis and molecular modelling of the antagonist SR 144528 binding site on the human cannabinoid CB(2) receptor. *Eur. J. Pharmacol.* 401, 17–25.
45. Ulfers, A. L., McMurtry, J. L., Kendall, D. A., and Mierke, D. F. (2002) Structure of the third intracellular loop of the human cannabinoid 1 receptor. *Biochemistry* 41, 11344–11350.
46. Mezei, M. (2004) SIMULAID: a collection of utilities designed to help setting up molecular simulations, New York.
47. Cherezov, V., Rosenbaum, D. M., Hanson, M. A., Rasmussen, S. G., Thian, F. S., Kobilka, T. S., Choi, H. J., Kuhn, P., Weis, W. I., Kobilka, B. K., and Stevens, R. C. (2007) High-resolution crystal structure of an engineered human {beta}2-adrenergic G protein coupled receptor. *Science* 318, 1258–1265, 5854.
48. Rasmussen, S. G., Choi, H. J., Rosenbaum, D. M., Kobilka, T. S., Thian, F. S., Edwards, P. C., Burghammer, M., Ratnala, V. R., Sanishvili, R., Fischetti, R. F., Schertler, G. F., Weis, W. I., and Kobilka, B. K. (2007) Crystal structure of the human beta(2) adrenergic G-protein-coupled receptor. *Nature* 450, 383–387.
49. Warne, T., Serrano-Vega, M. J., Baker, J. G., Moukhametzianov, R., Edwards, P. C., Henderson, R., Leslie, A. G., Tate, C. G., and Schertler, G. F. (2008) Structure of a beta1-adrenergic G-protein-coupled receptor. *Nature* 454, 486–491.
50. Altenbach, C., Kusnetzow, A. K., Ernst, O. P., Hofmann, K. P., and Hubbell, W. L. (2008) High-resolution distance mapping in rhodopsin reveals the pattern of helix movement due to activation. *Proc. Natl. Acad. Sci. U.S.A.* 105, 7439–7444.
51. McAllister, S. D., Rizvi, G., Anavi-Goffer, S., Hurst, D. P., Barnett-Norris, J., Lynch, D. L., Reggio, P. H., and Abood, M. E. (2003) An aromatic microdomain at the cannabinoid CB(1) receptor constitutes an agonist/inverse agonist binding region. *J. Med. Chem.* 46, 5139–5152.
52. Zhang, R., Reggio, P. H., and Song, Z.-H. (2004) Mutagenesis of aromatic microdomains at human CB2 cannabinoid receptor, in *2004 Symposium on the Cannabinoids*, International Cannabinoid Research Society, Paestum, Italy.
53. Nebane, N. M., Kellie, B., and Song, Z. H. (2006) The effects of charge-neutralizing mutation D6.30N on the functions of CB1 and CB2 cannabinoid receptors. *FEBS Lett.* 580, 5392–5398.
54. Shi, L., and Javitch, J. A. (2004) The second extracellular loop of the dopamine D2 receptor lines the binding-site crevice. *Proc. Natl. Acad. Sci. U.S.A.* 101, 440–445.

BI8007802